Determination of viscoelastic properties by analysis of probe-particle motion in molecular simulations

Mir Karim, Swapnil C. Kohale, Tsutomu Indei, Jay D. Schieber, and Rajesh Khare

Phys. Rev. E **86**, 051501 — Published 1 November 2012

DOI: 10.1103/PhysRevE.86.051501

Determination of Viscoelastic Properties by Analysis of Probe Particle Motion in Molecular Simulations

Mir Karim,[1] Swapnil C. Kohale,[1] Tsutomu Indei,[2] Jay D. Schieber,[2,3,a] and Rajesh Khare[1,b]

[1]Department of Chemical Engineering, Texas Tech University, Box 43121, Lubbock, TX 79409

[2]Department of Chemical and Biological Engineering and Center for Molecular Study of Condensed Soft Matter,

[3]Department of Physics,

Illinois Institute of Technology,

3440 S. Dearborn St., Chicago, Illinois 60616, U.S.A.

[a]email address: schieber@iit.edu

[b]email address: rajesh.khare@ttu.edu

Abstract

We present a technique for the determination of viscoelastic properties of a medium by tracking motion of an embedded probe particle by using molecular dynamics simulations. The approach involves analysis of the simulated particle motion by continuum theory; it is shown to work in both passive and active modes. We demonstrate that for passive rheology, an analysis based on the generalized Stokes-Einstein relationship (GSER) is not adequate to obtain the values of the viscoelastic moduli over the frequency range studied. For both passive and active modes, it is necessary to account for the medium and particle inertia when analyzing the particle motion. For a polymer melt system consisting of short chains, the values calculated from the proposed approach are in good quantitative agreement with previous literature results that were obtained using completely different simulation approaches. The proposed particle rheology simulation technique is general and could provide insight into the characterization of the mechanical properties in biological systems such as cellular environments and polymeric systems such as thin films and nanocomposites that exhibit spatial variation of properties over the nanoscale.

I. INTRODUCTION

Over the last two decades, particle microrheology has become established as an experimental technique for quantifying the relationship between particle motion in a complex medium and its microscale viscoelastic properties [1-3]. Going further down in length scale, the motion of nanoparticles in a viscoelastic medium plays an important role in many biological and physical processes. For example, diffusion of nanoparticles in sputum of cystic fibrosis patients [4] or in a living cancer cell [5] has been studied to develop nanoparticle-based drug delivery approaches, while nanoparticle diffusion towards human lung fibroblast cells in a cell culture is of interest [6] for the possible adverse effects of nanoparticle uptake by these cells. Straightforward extension of the bead microrheology approach for quantification of particle motion and viscoelastic properties at the nanoscale faces several challenges resulting from (1) the strong influence of the specific chemical interactions on the system behavior at these length scales, (2) the important role played by slip at the particle-medium interface, (3) the presence of structural heterogeneities in the system, as well as (4) the need to account for the expansion of the time scale i.e. frequency range that is necessary for nanoscale applications.

Molecular dynamics (MD) simulations possess the unique ability to account for these detailed chemical interactions as well as the structural heterogeneities in the system at the nanoscale. Previously molecular simulations in conjunction with Green-Kubo or non-equilibrium MD (NEMD) techniques have been used to determine the overall viscoelastic properties of the bulk polymer melt [7-9]. A technique for determining the local elastic modulus tensor from the second derivative of free energy with respect to strain has also been applied to polymeric systems [10]. However, these techniques do not allow for a systematic analysis of

particle motion in a viscoelastic medium and subsequent extraction of nanoscale viscoelastic properties. In this paper, we propose a molecular simulation approach analogous to the experimental particle microrheology technique for the determination of local viscoelastic properties at the nanoscale by analysis of particle motion in the medium of interest. This approach builds on our previous work which showed that molecular simulation results can be quantitatively analyzed using continuum mechanics expressions for a wide range of transport problems such as simple shear flow, oscillatory shear flow and thermal conduction [11, 12] as well as particle translation and rotation in a solvent medium [13, 14]. An important contribution of this work is the demonstration that both particle and medium inertia play a crucial role in governing system behavior at the time scales (frequency range) of interest in nanoscopic systems. We combine molecular simulations with a recent theoretical framework [15-17] to present a quantitative approach to account for these inertial effects in the system. Using this formalism, we demonstrate that the particle motion in a model polymer melt system can be analyzed to obtain the viscoelastic properties using both active and passive particle rheology approaches. The passive rheology formalism presented here can be used for analyzing the nanoparticle motion in biological systems [4-6] which is of interest for health science applications. On the other hand, the local viscoelastic properties obtained from the active particle rheology simulations can be used for characterizing spatial gradients in properties of heterogeneous systems such as polymer thin films and nanocomposites which is a difficult task experimentally [18].

II. MOLECULAR MODEL AND SIMULATION METHOD

The simulation system consists of a bulk polymer melt (coarse-grained chains with number of beads, $N = 20$) with a probe particle embedded in it. There are two kinds of beads in the system - beads comprising the probe particle and those constituting the polymer melt. A purely repulsive Lennard-Jones (LJ) potential, *i.e.,* the Weeks-Chandler-Andersen (WCA) interaction potential [19], is commonly used in rheology simulations. Our preliminary simulations indicated that usage of WCA interactions between the probe particle and the polymer melt lead to a large degree of slip at the particle surface which results in underestimation of viscoelastic moduli as determined from simulations. In our system, the beads of the probe particle interact with the beads of polymer chains via the full LJ potential with well depth $\varepsilon = 2.0$, and which is truncated at a distance of $r_c = 2.3\sigma$ (where σ is the molecular diameter); this was shown to effectively eliminate slip at the particle surface. All other atoms in the system interact via the WCA potential with $r_c = 2^{1/6}\sigma$ and $\varepsilon = 1.0$. All physical quantities are presented in reduced LJ units in the rest of the paper. A coarse-grained bead-spring model of the polymer chains is used where the chain beads are connected using the finitely extensible nonlinearly elastic (FENE) springs [20], $U_{FENE}(r) = -\frac{1}{2}KQ^2 \ln\left[1-\left(\frac{r}{Q}\right)^2\right]$ with spring constant $K = 30.0$ and the maximum allowable extension of the spring, $Q = 1.5$. Along with the WCA potential, this FENE model will prevent unphysical bond crossing between the chains. The probe particle is constructed by carving out a spherical region of nominal radius 2.5 from a face centered cubic lattice structure with lattice spacing 1.42. The integrity of the probe particle is maintained by connecting the neighboring constituent beads by stiff harmonic springs with a spring constant of

500. The MD simulations are carried out in a periodic cubic simulation box of edge length $L=150$ using the LAMMPS package [21]. The system density is kept at $\rho=0.85$ and the temperature is maintained at $T=1.0$ by using a Nosé-Hoover thermostat [22]. With this basic setup, both passive and active rheology simulations were carried out; a description of the analysis methodology for each follows along with the results.

III. ANALYSIS METHODOLOGY

In the standard experimental procedure for one-particle microrheology [1, 23], the dynamic modulus $G^*(\omega)$ of the medium is estimated from the particle's motion, which is assumed to obey the generalized Langevin equation (GLE)

$$m_{eff}\frac{d^2\boldsymbol{r}_b(t)}{dt^2}=-\int_{-\infty}^{t}\zeta(t-t')\frac{d\boldsymbol{r}_b(t')}{dt'}dt'+\boldsymbol{f}_{ex}(t)+\boldsymbol{f}_{\mathrm{B}}(t), \tag{1}$$

where $\boldsymbol{r}_b(t)$ is the particle position, m_{eff} is an appropriate particle mass, $\zeta(t)$ is the time-dependent friction, $\boldsymbol{f}_{ex}(t)$ is any external force and $\boldsymbol{f}_{\mathrm{B}}(t)$ is the Brownian random force on the particle. In the passive microrheology method, only Brownian motion is considered in the absence of external forces ($\boldsymbol{f}_{ex}(t)=0$). By using the fluctuation-dissipation theorem that relates the auto-correlation of $\boldsymbol{f}_{\mathrm{B}}(t)$ with $\zeta(t)$, and the generalized Stokes relation connecting the friction coefficient ζ with the dynamic modulus G^* in the frequency domain (taking account of medium inertia [15-17]), the GLE is transformed by a two-sided Fourier transform into [15]

$$\frac{6\pi RG^*(\omega)}{i\omega}+6\pi R^2\sqrt{\rho G^*(\omega)}+i\omega m_{eff}=Z^*(\omega), \tag{2}$$

where ρ is the medium density, R is the particle radius, and continuum mechanics suggests that the appropriate mass to use is the effective mass of the particle, *i.e.*, $m_{eff} = m_{bare} + \frac{2}{3}\pi R^3 \rho$, which consists of the bare particle mass (m_{bare}) plus the added mass from the medium. Eq. (2) is applicable for both passive and active rheology approaches, the only difference being that $Z^*(\omega)$, *i.e.* the friction on the particle traversing the viscoelastic medium, takes different forms in the two approaches. The first term on the left side of Eq. (2) is the generalized Stokes law for drag. The value of 6 for the coefficient assumes that the "no-slip" boundary conditions hold at the particle surface as discussed above. The second term is the Basset force [24], arising from medium inertia, which is a frictional force from the radiational dissipation of particle energy by elastic waves [17, 25]. The third term is the effective inertial force of the particle. The actual application of this formalism to passive and active particle rheology is described in what follows.

A. Passive rheology

For passive particle rheology, the quantity $Z^*(\omega)$ is given by $Z^*(\omega) \equiv Z^*_{passive}(\omega) := \frac{6k_B T}{(i\omega)^2 \overline{\langle \Delta r_b^2[\omega] \rangle}_{eq}}$. In this expression $\overline{\langle \Delta r_b^2[\omega] \rangle}_{eq}$ is the one-sided Fourier (or Laplace) transform of the mean-squared displacement (MSD) of the particle $\langle \Delta r_b^2(t) \rangle_{eq} = \left\langle \left[\boldsymbol{r}_b(t) - \boldsymbol{r}_b(0) \right]^2 \right\rangle_{eq}$, and k_B is the Boltzmann constant. By solving Eq. (2) for $\sqrt{G^*}$, we obtain the inertial generalized Stokes-Einstein relation (IGSER) that relates the dynamic modulus of the medium with the particle's MSD in the medium

$$G^*(\omega)=\frac{i\omega Z^*(\omega)}{6\pi R}+\frac{m_{eff}\omega^2}{6\pi R}+\frac{R^2\omega^2}{2}\left(\sqrt{\rho^2+\frac{2\rho}{3\pi R^3}\left(\frac{Z^*(\omega)}{i\omega}-m_{eff}\right)}-\rho\right). \quad (3)$$

The conventional inertia-less GSER: $G^*(\omega)=\frac{i\omega Z^*(\omega)}{6\pi R}$ is recovered by putting $m_{eff},\rho\to 0$ in the IGSER, Eq. (3).

In analogy with experiments, our passive particle rheology simulation approach consists of determining the viscoelastic properties of the model polymer melt by tracking the thermal motion of the probe particle embedded in it. Often, a local power-law is assumed to estimate the Laplace transform of MSD [23], and the approximate algebraic (inertia-less) GSER is used for data analysis [26]. This scheme is convenient, but the approximation is poor when the slope of the MSD varies rapidly and the power-law assumption is an oversimplification [23, 27]. Instead, we developed a more accurate method in which we fit and extrapolate the MSD data by using an appropriately smooth function that (i) is defined at all times $0\le t<\infty$, (ii) shows ballistic behavior $\left\langle \Delta r_b^2(t)\right\rangle_{eq}=Ct^2$ at the shortest-time regime, (iii) describes diffusive behavior $\left\langle \Delta r_b^2(t)\right\rangle_{eq}=6Dt$ at the longest-time regime, and (iv) is capable of being analytically Laplace transformed. There are several merits of choosing such a function: a truncation error resulting from a finite time window can be avoided; the MSD's behavior at the extrapolated ranges is physically natural; it avoids aliasing; and it saves calculation costs. We introduce a function $f^{(1)}(t)=1-\left(1+\frac{t}{\tau}\right)e^{-\frac{t}{\tau}}$ that shows ballistic behavior at $t<<\tau$ and gives a plateau at $t>>\tau$, and superpose a continuous spectrum of this function weighted with a power-law spectrum

$h(\tau)=\sum_{j=1}^{n} g_j \tau^{\alpha_j} H(\tau_j-\tau)H(\tau-\tau_{j-1})$ [28], where $H(\tau)$ is a unit step function, $\{\tau_j\}$ is a series of discrete relaxation times $(\tau_j > \tau_{j-1})$, and n is the number of modes of the spectrum. Usually one mode is sufficient to fit data for approximately two decades of time. By adding a second function $f^{(0)}(t)=e^{-\frac{t}{\lambda}}-1+\frac{t}{\lambda}$ that yields diffusive behavior at $t \gg \lambda$, our fitting function is

$$\left\langle \Delta r_b^2(t) \right\rangle_{eq} = \int_0^\infty \frac{h(\tau)}{\tau} f^{(1)}(t)\, d\tau + g_0 f^{(0)}(t). \tag{4}$$

We assume $\tau_n = \lambda$ without loss of generality. Our weights $\{g_j\}$ of the spectrum for all $j>1$ are determined from g_1 by enforcing a continuum condition for the weighting. Therefore the total number of free adjustable parameters $\{\alpha_1,...\alpha_n,\tau_0,...,\tau_{n-1},\lambda,g_0,g_1\}$ is $2n+3$. The diffusion coefficient D in the longest-time regime is obtained from Eq. (4) as $D=\frac{g_0}{6\lambda}$, indicating that g_0 is derived from λ once D is measured from the MSD data. Furthermore, g_1 can be derived from other parameters once the coefficient C of the ballistic motion is known from the data, because $C=\frac{g_1}{2}\sum_{j=1}^{n}\left(\prod_{k=1}^{j-1}\tau_k^{\alpha_k-\alpha_{k+1}}\right)\frac{\tau_j^{\alpha_j-2}-\tau_{j-1}^{\alpha_j-2}}{\alpha_j-2}+\frac{g_0}{2\lambda^2}$ as derived from Eq. (4).

B. Active rheology

As for active particle rheology, we again follow the approach of extracting medium transport properties by quantitative analysis of MD simulation results by continuum theory expressions. We performed active particle rheology simulation by subjecting the probe particle that is embedded in the polymer melt to an external force, similar to the experimental procedure

used by Ou-Yang and co-workers [29, 30]. The probe particle was held at a location using a harmonic trap with spring constant tensor $\boldsymbol{H}_{\mathrm{e}}$ ($H_{\mathrm{e},xx}=10$, $H_{\mathrm{e},yy}$, $H_{\mathrm{e},zz}=1000$, $H_{\mathrm{e},ij}=0$ for $i\neq j$) and also subjected to an oscillatory force along the x direction, i.e., $\boldsymbol{f}_{ex}(t)=\Re e\left\{Ae^{i\omega t}\right\}\mathbf{e}_x-\boldsymbol{H}_e.\boldsymbol{r}_b(t)$, where $\mathbf{e}_x$ is the unit vector along the x-axis, A is the amplitude, and $\boldsymbol{H}_{\mathrm{e}}$ is as described above. This external oscillatory force leads to an oscillatory motion of the particle; the ensemble-averaged x-component of the particle's deviation from the center of the oscillation can be expressed as: $\left\langle x_b(t)\right\rangle_{eq}=x_0(\omega)\,\Re e\left\{e^{i[\omega t-\delta(\omega)]}\right\}$, where $x_0(\omega)$ is the amplitude and $\delta(\omega)$ is the phase lag between the applied force and the particle displacement. By substituting this expression of $\left\langle x_b(t)\right\rangle_{eq}$ into the x-component of the ensemble-averaged GLE, i.e., Eq. (1) with $\boldsymbol{f}_{ex}(t)$ given above, and with the help of the generalized Stokes law, we obtain Eq. (2), but in this case $Z^*(\omega)$ is now set to $Z^*(\omega)\equiv Z^*_{active}(\omega):=\frac{1}{i\omega}\left(\frac{A}{x_0(\omega)}e^{i\delta(\omega)}-H_{\mathrm{e,xx}}\right)$.

Therefore G^* can be estimated from the particle motion measured through $x_0(\omega)/A$ and $\delta(\omega)$ by using the same equation as for passive rheology, i.e. Eq. (3).

IV. RESULTS

A. Passive rheology

The motion of the probe particle in the absence of an external force was tracked in passive rheology. Specifically, equilibrium MD simulations were carried out on the system for the

duration of 130 million time steps with time step 0.003. Simulations were carried out on ten different replicas of the system and the average MSD $\left\langle \Delta r_b^2(t) \right\rangle_{eq}$ of the center of mass of the

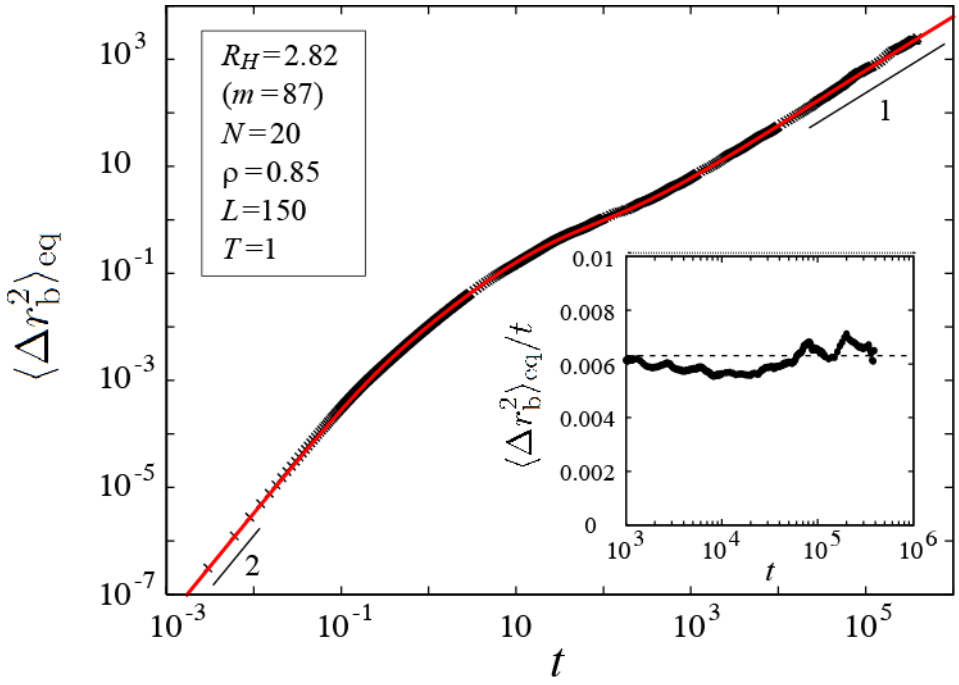

FIG. 1. (Color online) The equilibrium averaged mean squared displacement of the simulated particle. Solid line shows fit to MSD data obtained by setting the adjustable parameters in Eq. (4) to $n = 4, \alpha_1 = 1.34, \alpha_2 = 0.42, \alpha_3 = 0.99, \alpha_4 = 0.6,\ \tau_0 = 0.13, \tau_1 = 7.8, \tau_2 = 105,\ \tau_3 = 7100, \tau_4 = \lambda = 10^4,$ and $g_1 = 0.0125$.

probe particle was determined from these. Figure 1 shows the MSD of a particle embedded in a polymer melt with N = 20. The hydrodynamic radius of the particle is estimated to be $R_H = 2.82$ from the first peak of the radial distribution function of the monomer beads around the center of mass of the nanoparticle [14]. The bare particle mass and (apparent) density of the nanoparticle are $m_{bare} = 87.0$ and $\rho_b = 0.93$, respectively. We use continuum expressions to analyze the MD simulation results; this tacitly assumes that the nanoparticle sees the polymer

melt as a continuum, even though our nanoparticle is only 30% larger than the polymer chains, whose radius of gyration, R_g is 2.16. We note that it has recently been pointed out [31] that particle motion in unentangled polymer melts conforms with Stokes-Einstein diffusion, provided the particle size is about 1.5 times the polymer chain size.

Also seen from the figure, four modes are sufficient to fit the data for the whole range. The fitting result is shown in Fig. 1. From the mean value of $\frac{\left\langle \Delta r_b^2(t) \right\rangle_{eq}}{t}$ for $t > 10^4 \left(= \lambda\right)$ the diffusion coefficient is estimated as $D = 0.0011$ (see inset of Fig. 1). At very short times (t < 0.01), the slope of the logarithmic MSD approaches 2.0 (it is between 1.99 and 2.00 for t < 0.01), as is expected for the ballistic regime. Using these short time MSD data, the ballistic coefficient is estimated from the mean value of $\frac{\left\langle \Delta r_b^2(t) \right\rangle_{eq}}{t^2}$ for $t < 0.01$ as $C = 0.0346$. Combining this result with the IGSER prediction of $\left\langle \Delta r_b^2(t) \right\rangle_{eq} \approx Ct^2$ in the ballistic regime, where $C = \frac{3k_BT}{m_{observed}}$, the mass of the particle is estimated to be $m_{observed} = 86.7$ from the fit of the ballistic regime. This value of particle mass is very close to the bare particle mass value of $m_{bare} = 87$, rather than the effective particle mass value which can be estimated to be: $m_{bare} + \frac{2}{3}\pi R_H^3 \rho = 126.6$ (or $m_{bare} + \frac{2}{3}\pi R^3 \rho = 114.5$). This observation can be quantitatively rationalized as follows: if one assumes that the difference between the effective and bare mass of the particle (i.e. the added mass) is contained in a shell of thickness L_s around the moving particle, then the value of L_s can be estimated as

$$\frac{2}{3}\pi R_{particle}^3 = \frac{4}{3}\pi\left(\left(R_{particle} + L_s\right)^3 - R_{particle}^3\right)$$

This suggests that $L_s = \left[\left(\frac{3}{2}\right)^{\frac{1}{3}} - 1\right] R_{particle} \sim 0.1447 R_{particle} \sim 0.41\sigma$ (using $R_{particle} = 2.82\sigma$).

We believe that the value of L_s so calculated is the smallest length scale involved in the continuum approximation. Since the value of L_s as estimated above is even smaller than the size of the medium beads, the assumptions underlying this length scale and hence the added mass concept of continuum theory, break down for the discrete nanoscale systems as illustrated by the analysis of the MSD data in the ballistic regime here. The value of particle mass that is calculated from the MSD data in the ballistic regime $m_{observed} = 86.7$ is used in our analysis for the calculation of $G^*(\omega)$.

In Fig. 2, the dynamic moduli of the polymer melt estimated from the bead's MSD via the IGSER and GSER are compared with literature values for $G^*(\omega)$ that were obtained from NEMD [7, 9] and equilibrium MD using the Green-Kubo relation [8]. The dynamic modulus derived from the IGSER agrees with the results from NEMD up to $\omega \lesssim 1$, whereas that from the inertia-less GSER cannot capture the high frequency behavior of $G^*(\omega)$ mainly due to the absence of medium inertia ($G'(\omega)$ even becomes negative in this case). In the terminal zone, $G^*(\omega)$ estimated from both IGSER and GSER agrees with the results of NEMD [9] rather than with the results from the Green-Kubo approach [8], probably because of larger statistical errors from shorter simulation times in the latter method.

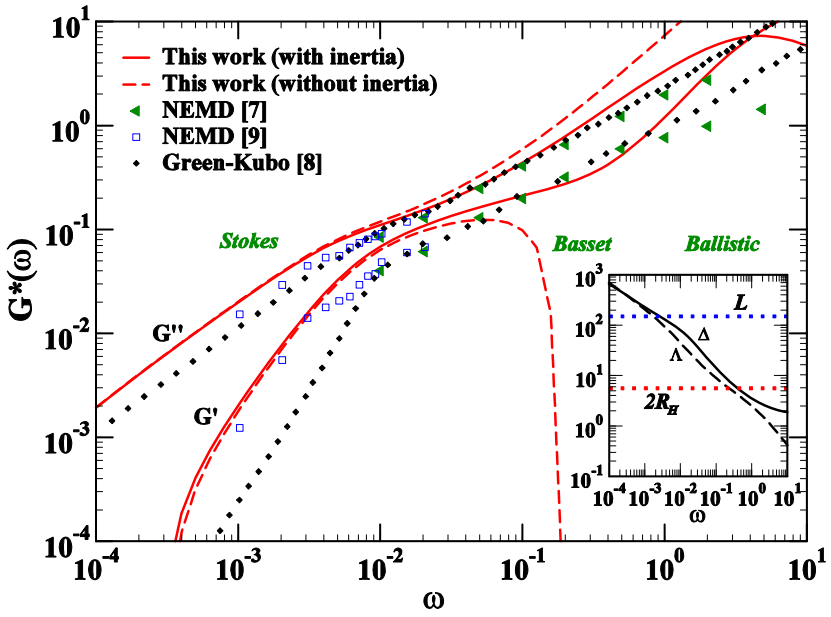

FIG. 2. (Color online) Comparison of G' and G'' derived from the MSD data presented in Fig. 1 (solid lines include inertial effects while dashed lines do not) with literature data (symbols). Inset: The penetration depth (Δ), and the wavelength (Λ) of the elastic wave propagating in the medium as a function of frequency.

It is important to determine the frequency range over which IGSER can be applied for a given simulation system. Two characteristic length-scales are important in viscoelastic materials: the penetration-depth $\Delta = \frac{|G^*|}{\omega}\sqrt{\frac{2}{\rho\left(|G^*|+G'\right)}}$ and the wave-length $\Lambda = \frac{|G^*|}{\omega}\sqrt{\frac{2}{\rho\left(|G^*|-G'\right)}}$ [17] of the shear wave, both of which are typically decreasing functions of ω. In the low-frequency regime ($\omega<0.001$) where the penetration-depth Δ is comparable to the distance $L-2R$ between the surfaces of the particle and its image in the simulations, the elastic wave does not decay before reaching the particle's periodic image in the neighboring box. This leads to unreliable results for the MSD of the particle thus giving a poor estimate of the bulk rheology of the medium (the simulation setup acts more like two- or multi-particle microrheology in that

case). In our simulations, L = 150, so data are reliable only when $\omega \gtrsim 0.001$ (see inset Fig. 2). On the other end of the frequency range, with increasing ω, the Basset force becomes gradually effective, and becomes dominant when Λ becomes smaller than the particle size (see inset of Fig.2). At the ultra-high frequencies where the third term of Eq. (2) is dominant, the particle motion is ballistic $\left\langle \Delta r_b^2(t) \right\rangle_{eq} = \frac{3k_B T}{m_{observed}} t^2$, which is independent of the medium viscoelasticity. Although this contribution can be subtracted out in theory, the signal-to-noise ratio becomes too poor to extract $G^*(\omega)$ for these frequencies. More importantly, for $\omega \gtrsim 3$, the wavelength Λ becomes smaller than the size of the medium bead σ (=1), and the continuum treatment on which our analysis is based is expected to break down at these conditions. In fact, one could argue that $G^*(\omega)$ as defined by the macroscopic stress ceases to be meaningful at these frequencies, whereas the microscopic Green-Kubo expression might hold.

B. Active rheology

For active rheology, the probe particle was put in a harmonic trap and its motion under the influence of an external oscillatory force was tracked using MD simulations. We performed simulations at different values of frequency spanning the range $0.002 \le \omega \le 0.1$; based on arguments presented for the passive rheology case, we expect the G' and G'' values to be reliable in this range. The amplitude A of the external force was adjusted in each of these cases to maintain the particle displacement amplitude $x_0(\omega)$ between 1.2 and 1.4. This range is chosen so that the displacement amplitude is smaller than the particle size, yet sufficiently large to obtain a good signal. The simulations consisted of an equilibration stage of at least 20 (40) periods followed by a production stage, where the particle was tracked, of at least 30 (60) periods

for frequencies lower (higher) than 0.01. The absence of higher harmonics was verified by taking the Fourier transform of these data and checking for the occurrence of only a single peak. Values of G', G'' were then obtained from Eq. (3). Here we note that a naïve application of Eq. (3) will entail using effective mass of the particle, m_{eff}, however, in light of the results for passive rheology described above, we used the observed particle mass, $m_{observed}$ ($\sim m_{bare}$) in these calculations.

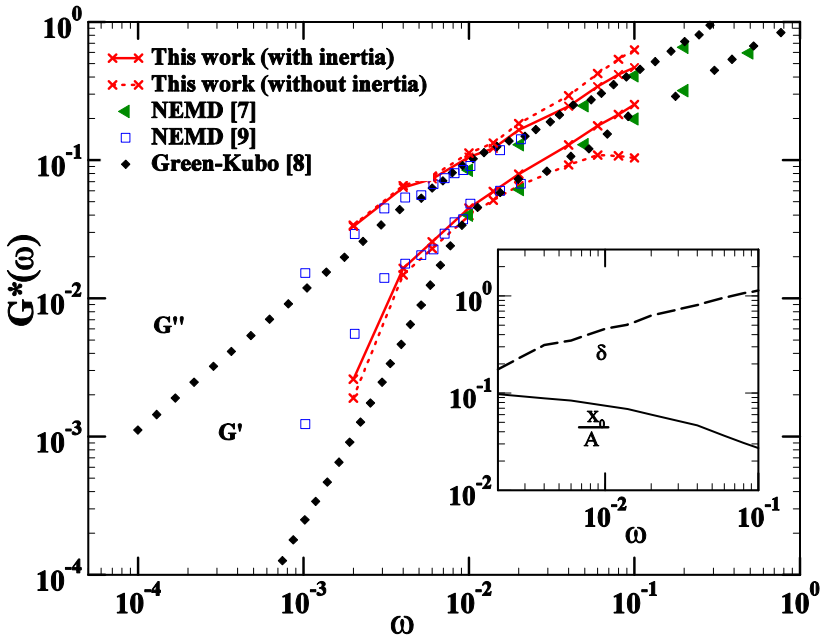

FIG. 3. (Color online) Comparison of $G^{'}$ and $G^{''}$ from active particle rheology simulations (solid lines include inertial effects while dashed lines do not) with literature data (symbols). Inset: The phase shift and the amplitude of the particle displacement.

Figure 3 shows that the $G''(\omega)$ values calculated from active rheology simulations show good quantitative agreement with previous literature data over the entire frequency range studied. Our $G'(\omega)$ values calculated by accounting for inertia agree with the literature data for $\omega \gtrsim 0.01$. At frequencies lower than 0.01, similar to the passive particle rheology case, our

values tend to agree with the NEMD results of Vladkov et al. [9], although the value at the lowest frequency shows a small deviation from the literature result, perhaps because of the low signal to noise ratio due to the usage of a smaller number of oscillation periods for averaging at the lower frequencies.

V. CONCLUSIONS

In summary, we have presented a particle rheology technique in both active and passive modes that combines molecular simulations with continuum theory to yield viscoelastic properties of a medium by analysis of probe particle motion in it. The analysis is facilitated by elimination of slip at the particle-medium interface. More importantly, we have shown that for the frequency range of interest to nanoscale systems, both medium and particle inertia play a crucial role in governing probe-particle motion in the complex medium. We have also carried out a detailed analysis of the wave propagation in the medium to determine the frequency range over which reliable results can be obtained from the analysis presented here; these predictions were verified by the actual simulation values. Although the particle rheology approach is being increasingly applied in experimental work, apparently, this is the first implementation of particle rheology approach in molecular simulations for the calculation of viscoelastic properties of a complex fluid. The molecular simulation approach presented here can be used for analyzing particle motion in complex viscoelastic media such as biological systems, where specific chemical interactions significantly influence the system behavior. The technique can also be readily extended for mechanical characterization of nanoscale heterogeneities in systems (e.g. polymer thin films, polymer nanocomposites) that exhibit spatial variation of properties over nanoscopic length scales.

Acknowledgments: Authors thank Andrés Córdoba for insightful discussions. We acknowledge partial financial support of this work by 3M (3M Non-Tenured Faculty Grant, to RK) and Army Research Office (Grants: ARO W911NF-09-2-0071 and W911NF-11-2-0018, to JDS). The majority of MD simulations were carried out on a computational cluster supported by CRIF MU instrumentation grant (Grant: NSF CHE-0840493) from National Science Foundation.

References

[1] T. Mason, and D. Weitz, Phys. Rev. Lett. **74**, 1250 (1995).
[2] D. Chen, E. R. Weeks, J. C. Crocker, M. F. Islam, R. Verma, J. Gruber, A. J. Levine, T. C. Lubensky, and A. G. Yodh, Phys. Rev. Lett. **90**, 108301 (2003).
[3] T. Squires, and J. Brady, Phys. Fluids **17**, 073101 (2005).
[4] J. S. Suk, S. K. Lai, Y. Wang, L. M. Ensign, P. L. Zeitlin, M. P. Boyle, and J. Hanes, Biomaterials **30**, 2591 (2009).
[5] W. Sun, N. Fang, B. G. Trewyn, M. Tsunoda, I. I. Slowing, V. S. Y. Lin, And E. S. Yeung, Anal. Bioanal. Chem. **391**, 2119 (2008).
[6] L. K. Limbach, Y. Li, R. N. Grass, T. J. Brunner, M. A. Hintermann, M. Muller, D. Gunther, and W. J. Stark, Environ. Sci. Technol. **39**, 9370 (2005).
[7] J. Cifre, S. Hess, and M. Kröger, Macromol. Theory Simul. **13**, 748 (2004).
[8] S. Sen, S. Kumar, and P. Keblinski, Macromolecules **38**, 650 (2005).
[9] M. Vladkov, and J.-L. Barrat, Macromol. Thoery Simul. **15,** 252 (2006).
[10] K. Yoshimoto, T. S. Jain, K. V. Workum, P. F. Nealey, and J. J. de Pablo, Phys. Rev. Lett. **93**, 175501 (2004).
[11] R. Khare, J. J. de Pablo, and A. Yethiraj, J. Chem. Phys. **107**, 2589 (1997).
[12] R. Khare, J. J. de Pablo, and A. Yethiraj, J. Chem. Phys. **114**, 7593 (2001).
[13] S. Kohale, and R. Khare, J. Chem. Phys. **129**, 164706 (2008).
[14] S. Kohale, and R. Khare, J. Chem. Phys. **132**, 234706 (2010).
[15] T. Indei, J. D. Schieber, A. Córdoba, and E. Pilyugina, Phys. Rev. E **85**, 021504 (2012).
[16] A. Córdoba, T. Indei, and J. Schieber, J. Rheol. **56**, 185 (2012).
[17] T. Indei, J. D. Schieber, and A. Córdoba, Phys. Rev. E, **85**, 041504 (2012).
[18] C. J. Ellison, and J. M. Torkelson, Nat. Mater. **2**, 695 (2003).
[19] J. D. Weeks, D. Chandler, and H. C. Anderson, J. Chem. Phys. **54**, 5237 (1971).
[20] H. R. Warner Jr., Ind. Eng. Chem. Fundam. **11**, 379 (1972)
[21] S. Plimpton, J. Comput. Phys. **117**, 1 (1995).
[22] W. Shinoda, M. Shiga, and M. Mikami, Phys. Rev. B **69**, 134103 (2004).
[23] T. Mason, Rheol. Acta **39**, 371 (2000).
[24] G. G. Stokes, Trans. Cambridge Philos. Soc. **9**, 8 (1856).
[25] M. Grimm, S. Jeney, and T. Franosch, Soft Matter **7**, 2076 (2011).
[26] T. Mason, K. Ganesan, J. H. van Zanten, D. Wirtz, and S. C. Kuo, Phys. Rev. Lett. **79**, 3282 (1997).
[27] B. Dasgupta, S. Tee, J. C. Crocker, B. J. Frisken, and D. A. Weitz, Phys. Rev. E **65**, 051505 (2002).
[28] M. Baumgaertel, A. Schausberger, and H. Winter, Rheol. Acta **29**, 400 (1990).
[29] L. Hough, and H. Ou-Yang, J. Nanopart. Res **1**, 495 (1999).
[30] M. Valentine, L. Dewalt, and H. Ou-Yang, J. Phys.: Condens. Matter **8**, 9477 (1996).
[31] U. Yamamoto, and K. S. Schweizer, J. Chem. Phys. **135**, 224902 (2011).